Precipitation Hardening in Nickel-Copper Base Alloy Monel K 500

G.K. DEY, R. TEWARI, P. RAO, S.L. WADEKAR, and P. MUKHOPADHYAY

The occurrence of a significant amount of age hardening, due to the precipitation of the γ' phase, has been demonstrated in the nickel-copper base alloy MONEL K 500. The microstructure of the precipitation-hardened and deformed alloy has been examined in peak-aged underaged and overaged conditions. An attempt has been made to compare the observed increments in strength in these three aged conditions to those predicted on the basis of relevant theoretical models.

I. INTRODUCTION

MONEL* K 500 is a nickel-base age-hardenable alloy containing a substantial amount of copper together with small amounts of iron, manganese, aluminum, and titanium. Age hardening in this alloy is caused by the formation of coherent, ordered ($Ni_3(Al, Ti)$) precipitates.[1] This alloy not only possesses excellent corrosion resistance like other monel alloys but also has a high room-temperature strength, comparable to those of some Ni-Cr-base alloys and low-alloy precipitation hardening steels.

*MONEL is a trademark of Inco Alloys International, Inc., Huntington, WV.

Although this alloy has been in use for some time, its age-hardening behavior does not appear to have been studied in detail previously. This article describes the age-hardening response of MONEL K 500 and attempts a systematic analysis of the relationship between the microstructure of the alloy and its strength. The microstructure has been studied with special reference to the dislocation arrangements and the dislocation-precipitate interactions in specimens containing different volume fractions and sizes of precipitates. An effort has been made to compare the observed increase in strength due to precipitation with that predicted theoretically on the basis of the available models. MONEL K 500, like some other commercial, nickel-base, precipitation-hardenable alloys (e.g., NIMONIC* PE16 and NIMONIC 105), is well suited for a comparative study of this kind, since the ordered phase forms as coherent, nearly stress-free (zero misfit), spherical precipitates. These particles, after isothermal aging treatments, cover a wide range of precipitate sizes. In the present work, the theoretical increase in strength in the underaged condition has been estimated by a combination of the Brown–Ham[2] and the Haasen–Labusch models.[3] In the peak-aged and slightly overaged conditions, a theoretical estimate of the increase in strength has been obtained on the basis of the formulation proposed by Nembach and Neite.[4] For significantly overaged conditions, the relationship suggested by Kocks[5] and Hirsch and Humphrey[6] has been used. While analyzing the experimental data, the anisotropy of the matrix has been taken into account. The dislocation line tension has been evaluated with respect to its dependence on the size and volume fraction of the particles. Loss of solid solution strengthening of the solute-depleted matrix in the aged specimens has been taken into account while determining the strengthening contribution of the precipitates. The effect of precipitates on fracture morphology has been also discussed.

*NIMONIC is a trademark of Inco Alloys International, Inc., Huntington, WV.

G.K. DEY, R. TEWARI, S.L. WADEKAR, and P. MUKHOPADHYAY, Scientific Officers, are with the Metallurgy Division, Bhabha Atomic Research Centre, Trombay, Bombay 400 085, India. P. RAO, Graduate Student, is with the Department of Metallurgical Engineering, Indian Institute of Technology, Kharagpur 721 302, India.

Manuscript submitted January 12, 1993.

II. EXPERIMENTAL

The MONEL K 500 alloy used in this work was obtained from International Nickel Company Ltd. in sheet form. The nominal composition of the alloy is given in Table I. Cold-rolled sheets of thickness 1.5 mm were used for making tensile specimens. Room-temperature tensile tests were carried out using an Instron tensile testing machine at a strain rate of 10^{-3}/s.

Solution treatment of specimens was carried out at 1223 K for 1 hour, followed by water quenching. Aging was carried out at 873, 923, and 973 K for periods ranging from a few hours to several days, followed by water quenching. For all these heat treatments, the specimens were encapsulated in evacuated silica capsules, containing helium gas at 175-mm pressure. Specimens for transmission electron microscopy were prepared by jet electropolishing, using an electrolyte containing 33 pct nitric acid and 67 pct methanol by volume. The electrolyte temperature was maintained at about 240 K.

III. RESULTS

A. *Microstructural Studies*

1. *Microstructure of the undeformed alloy*

The solution-treated specimens consisted of austenite (γ) grains, the average size being about 5 μm. Some of the grains were found to contain annealing twins (Figure 1(a)). Blocky particles of a TiC-type primary

Table I. Nominal Composition of the Alloy

Element	Ni	Mn	Fe	Si	Cu	Al	Ti
Amount (wt pct)	61.80	1.25	2	1	30.20	3.5	0.95

carbide phase were distributed in intergranular as well as intragranular locations (Figures 1(b) and (c)). Electron diffraction observations failed to indicate the presence of any state of order (long range or short range) in the γ phase.

The formation of γ' precipitates was studied in solution-treated and aged specimens. The precipitates had a spherical morphology (Figure 2). The distribution of the γ' particles was homogeneous, and the grain boundaries did not show any precipitate-depleted regions. However, precipitate-depleted regions were often observed around the TiC-type carbide particles. Precipitates of an $M_{23}C_6$-type phase were found to form at the grain boundaries in the aged specimens. These precipitates had a plate-shaped morphology and did not appear to join to form a continuous layer along the γ grain boundaries (Figure 3).

The volume fraction of the γ' phase was found by electron microscopy to be approximately 6.5 pct at the aging temperature of 923 K. The misfit, ε, defined as $(a' - a)/a$ (where a' is the lattice parameter of the γ' phase and a is the lattice parameter of the γ phase) was determined from X-ray diffraction to be about 0.05 pct. The misfit was also determined by convergent beam electron diffraction (CBED). Figure 4 shows a CBED pattern corresponding to the [111] zone axis in a specimen aged at 873 K for 16 hours. Due to the small size of the precipitates, the pattern has superposition of higher order Laue zone (HOLZ) lines from the precipitate as well as from the matrix, manifested in the form of a splitting of the HOLZ lines. A comparison of the observed HOLZ lines with the simulated patterns revealed that the lattice parameter mismatch is less than 5×10^{-13} m (0.005 Å). A description of the microstructure of the solution-treated alloy and of the γ' precipitation kinetics has been published elsewhere.[1]

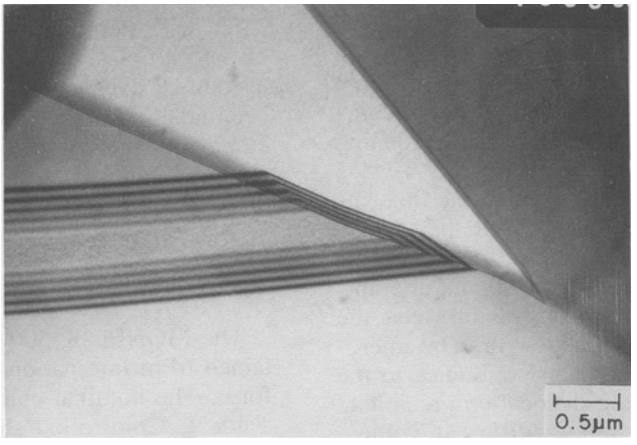

(*a*)

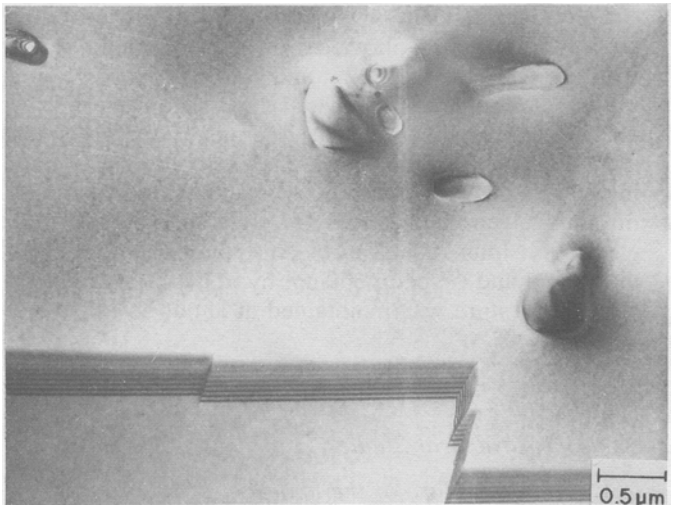

(*b*)

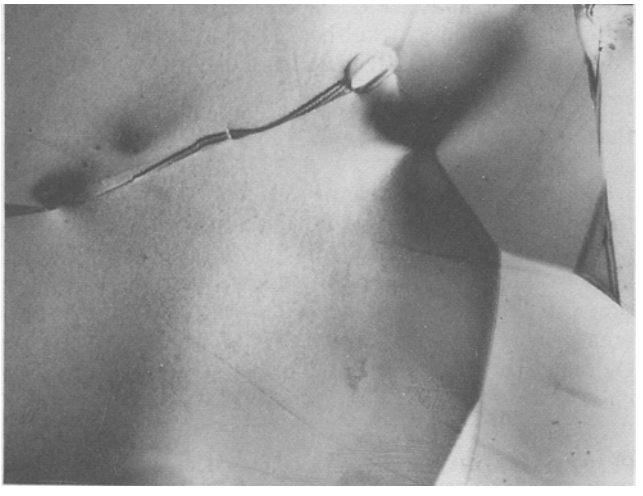

(*c*)

Fig. 1—Bright-field electron micrographs showing (*a*) annealing twins in the solution-treated specimens and (*b*) intragranular and (*c*) intergranular distribution of TiC-type primary carbide phase.

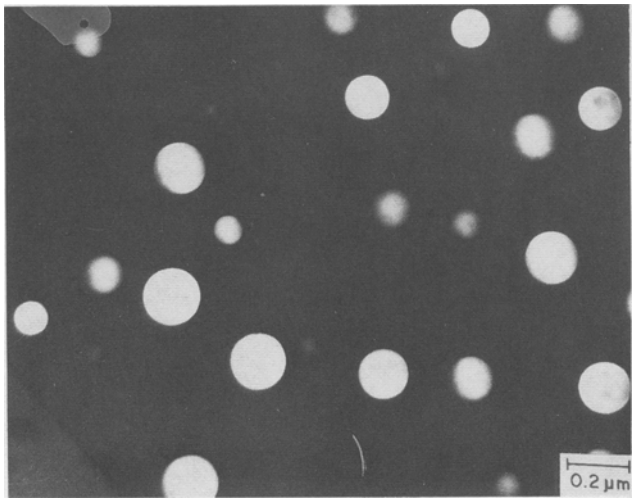

Fig. 2—Dark-field micrograph showing spherical $Ni_3(Ti, Al)$ precipitates in the solution-treated and aged specimen (973 K for 1000 h).

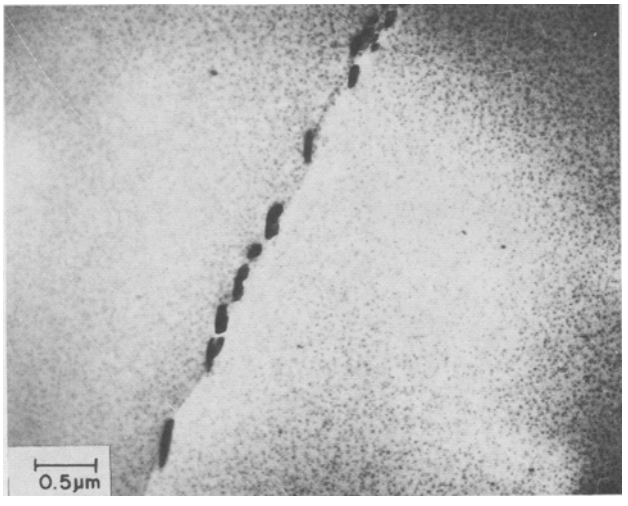

Fig. 3—Precipitates of the $M_{23}C_6$-type carbide phase at the grain boundaries.

2. *Microstructure of the deformed alloy*

The arrangement of dislocations in the solution-treated and deformed (3 pct deformation) specimens was found to be nonplanar in several regions of the grains. Dislocation tangles could be observed clearly (Figure 5(a)). The absence of any marked tendency of the dislocations, either for distribution along well-defined planar arrays or for pairing, was suggestive of the fact that the stacking fault energy of the alloy was not low and that short-range order was absent in the solution-treated and water-quenched material. In the context of stacking fault energy, it could be mentioned here that although nickel has a high stacking fault energy,[7] alloying may decrease the value of this parameter, as has been noted, for instance, for many Ni-Cr-base alloys.[8] Though copper is present in MONEL K 500 in a substantial quantity, its addition is not very effective in reducing the stacking fault energy of nickel.[9] The change in stacking fault

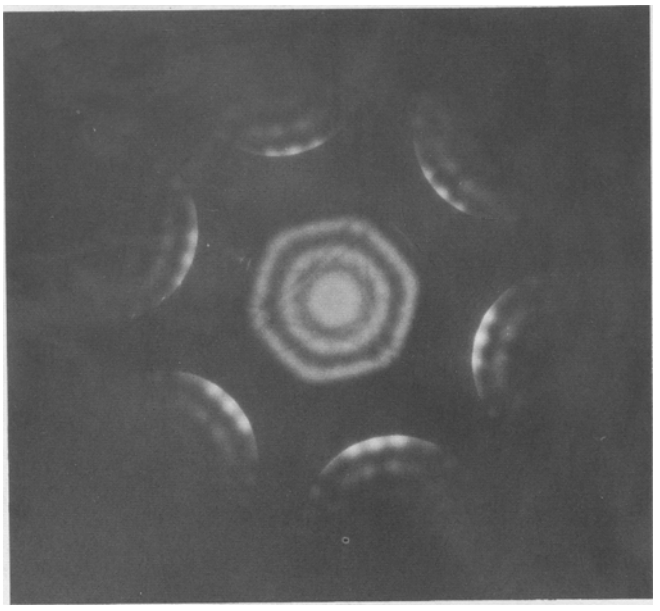

Fig. 4—CBED pattern from the {111} zone axis in specimen aged at 873 K for 16 h.

energy of the Ni-Cu matrix in this alloy, due to the other alloying additions, is very likely to be very small due to the fact that these elements are present in small quantities. It is pertinent to mention in this context that Raynor and Silcock,[10] in their studies on some γ'-hardened alloys, have observed tangled dislocation arrangements in the solution-treated and deformed condition and have attributed such arrangements to the high stacking fault energy of the alloy.

Solution-treated specimens, after aging at 973 K for 2 hours, showed a planar arrangement of dislocations in most of the regions (Figure 5(b)). The occurrence of superlattice reflections in selected area diffraction patterns indicated that precipitation had occurred as a result of this aging treatment. Most of the planar dislocation arrays were found to emanate from the grain boundaries. This kind of dislocation arrangement is indicative of the occurrence of inhomogeneous slip and is typical of many precipitation-hardened alloys.[11] In these alloys, dislocations can shear the particles and move through them when the small interparticle spacing does not permit by-passing the particles by looping. The formation of sharp slip bands occurs, since the shearing of particles leads to a lowering of the resistance against further dislocation motion in the slip planes.[12]

In specimens containing precipitates, the dislocations showed a tendency for pairing (Figure 6). Movement of dislocations in pairs has been observed in many ordered alloys.[13] The movement of the leading dislocation creates disorder in the ordered particle, which is subsequently restored by the movement of the trailing dislocation.

The dislocation arrangement continued to be planar in specimens containing larger precipitates (precipitate size ~10 nm). Dark-field micrographs (Figure 7) indicated a displacement of the two halves of a precipitate due to the shearing action of the dislocations. As the precipitate size increased further, a qualitative change

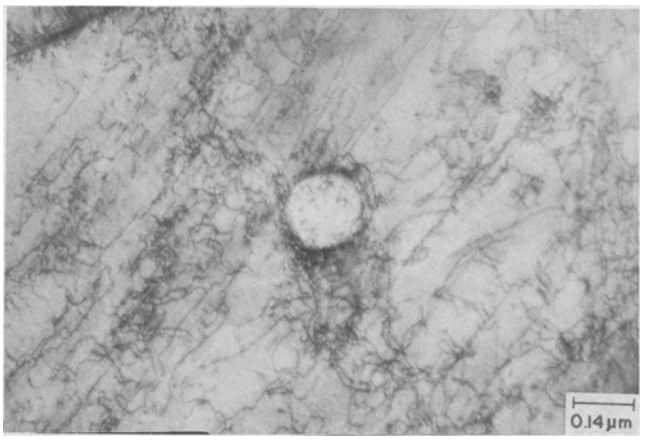

(*a*)

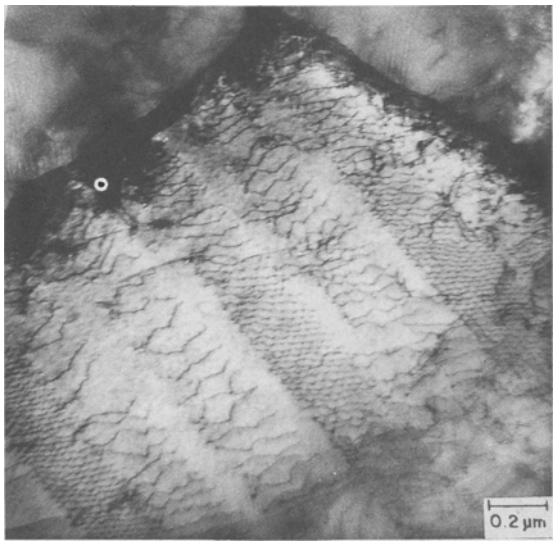

(*b*)

Fig. 5—Bright-field electron micrographs showing (*a*) tangled dislocation arrangement in solution-treated alloy and (*b*) planar arrangement of dislocations in solution-treated and aged specimen (973 K for 2 h).

Fig. 6—Planar arrangement of dislocation pairs in specimen aged at 873 K for 2 h.

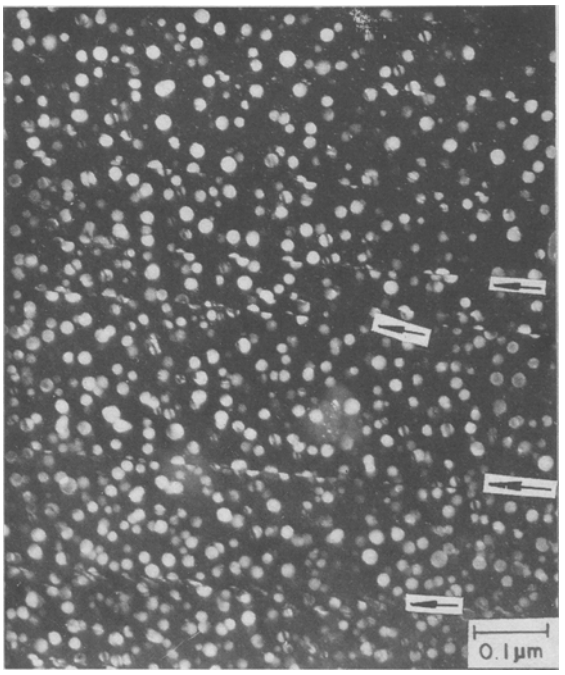

Fig. 7—Dark-field micrograph indicating the displacement of the two halves of γ′ precipitates (shown by arrows) due to the shearing action of the dislocations.

was found to occur in the arrangement of dislocations. Well-defined planar arrays were no longer observable. Instead, complex dislocation bands could be seen (Figure 8(a)). The dislocation arrangement in these complex bands was suggestive of the fact that direct interaction had occurred between dislocations on a number of slip planes. With further increase in precipitate size (precipitate size 20 nm; specimen aged at 973 K for 64 hours), more changes were observed in the dislocation arrangement as well as in the nature of dislocation-precipitate interaction. Though the dislocation arrangement was predominantly planar in specimens containing very small precipitates, as the precipitate size increased, the leading dislocations in dislocation pairs started showing a marked tendency for bowing (Figure 8(b)). With a further increase in the precipitate size, it was possible to see loops along with the slip bands (Figure 9). Weak beam images indicated that though bandlike features were present, dislocations had actually started forming tangles (Figure 10). Secondary slip interactions could be observed in some instances (Figure 11(a) and (b)). In substantially overaged specimens, Orowan looping was found to be the predominant mode of dislocation-precipitate interaction (Figure 12). The occurrence of more than one loop could also be observed around some particles. Intersection of loops on two intersecting slip planes, leading to the formation of ⟨100⟩ dislocation segments, has been observed by Singhal and Martin.[14] In Figure 12, loops which are parallel to the plane of the figure (marked A) can be seen, as well as those which are perpendicular to this

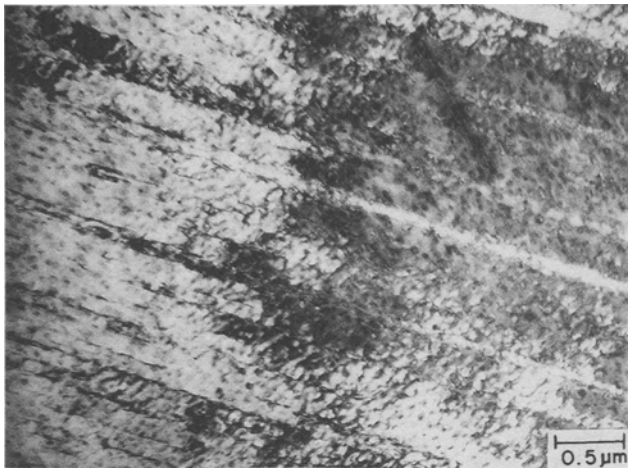

(*a*)

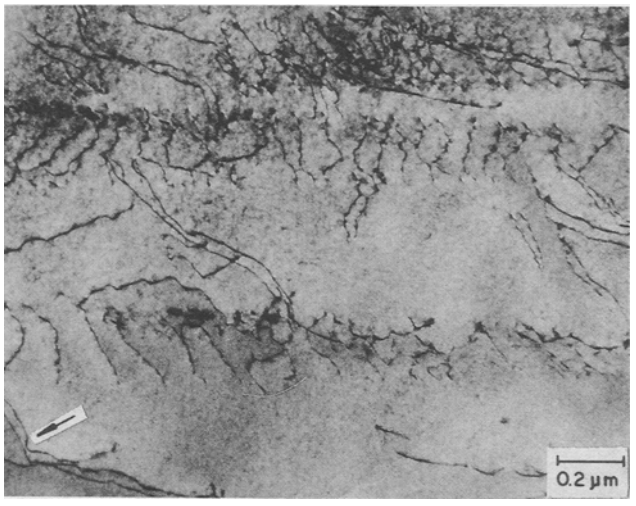

(*b*)

Fig. 8—(a) Bright-field image of complex dislocation bands and (*b*) the bowing tendency of the leading dislocation in pairs (shown by arrow).

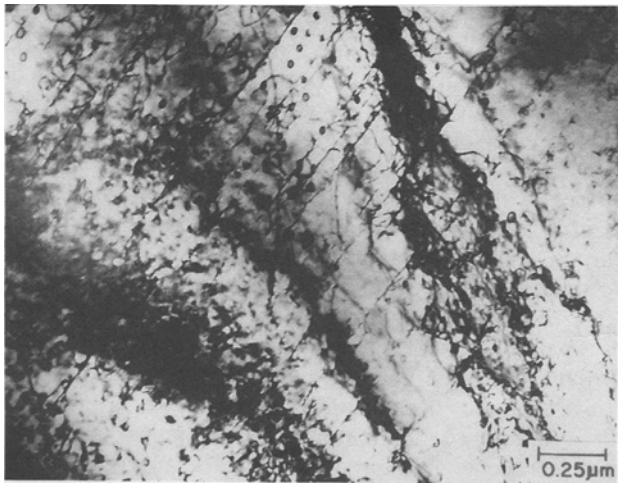

Fig. 9—Bright-field image of loops along with slip bands in specimen aged at 973 K for 16 h.

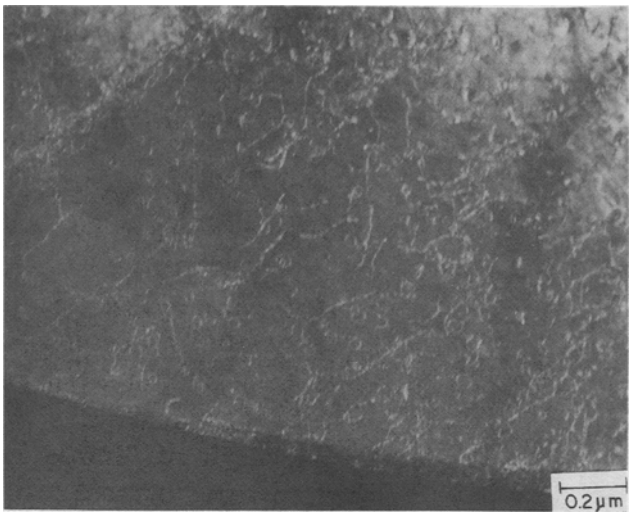

Fig. 10—Weak beam image showing dislocation tangles in specimen aged at 973 K for 16 h.

plane (marked B). Intersection of such loops is likely to lead to the formation of sessile dislocations of the ⟨100⟩ type and to result in rapid work hardening.[14]

B. *Strength Evaluation*

The effects of aging time and temperature on the hardness and yield strength of the alloys were studied. The variation in hardness with aging time at different temperatures is shown in Figure 13(a). The hardness increased monotonically with increasing aging time at the aging temperature of 873 K and saturated after about 64 hours of aging. However, a drop in hardness was observed after relatively small periods at higher temperatures (923 and 973 K) due to overaging. The dependence of the yield strength on the aging parameters was found to follow a trend similar to that of the hardness (Figure 13(b)). The observed increase in flow stress has been compared with the theoretically estimated values in Section IV–B.

C. *Fractography*

In solution-treated specimens, the fracture surface was found to consist of deep dimples (Figure 14(a)) with a bimodal size distribution. The larger dimples had a number density similar to those of the primary carbides. Moreover, carbide particles were found to be embedded at the base of some of these dimples. These observations were suggestive of the fact that the primary carbides act as nucleation sites for voids. The smaller dimples, the majority of which were found to lie on the ridges of the larger dimples, might have originated at smaller inclusions which could not be identified by microstructural examination. Thompson and Weihrauch[15] have postulated the presence of these inclusions to explain dimple formation in relatively clean metallic materials.

In specimens containing very small- (<10 nm) and intermediate-sized (≈15 nm) γ' particles, large dimples with carbide particles could be seen. These dimples were found to be shallower, indicating a smaller ductility at

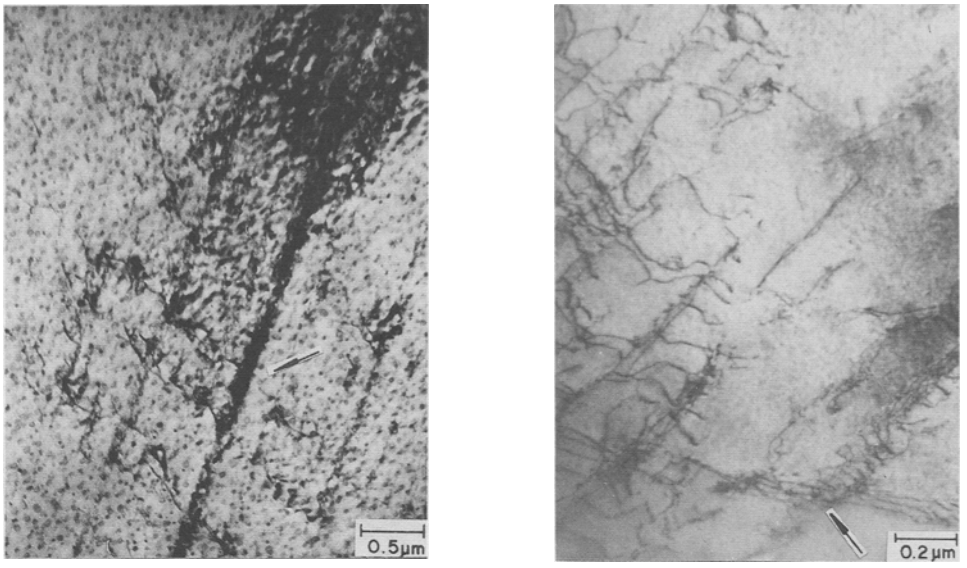

(*a*) (*b*)

Fig. 11—Bright-field electron micrographs showing interaction between dislocations (indicated by arrows) lying on (*a*) ($\bar{1}11$) and ($1\bar{1}1$) and (*b*) ($1\bar{1}1$) and ($11\bar{1}$) slip planes.

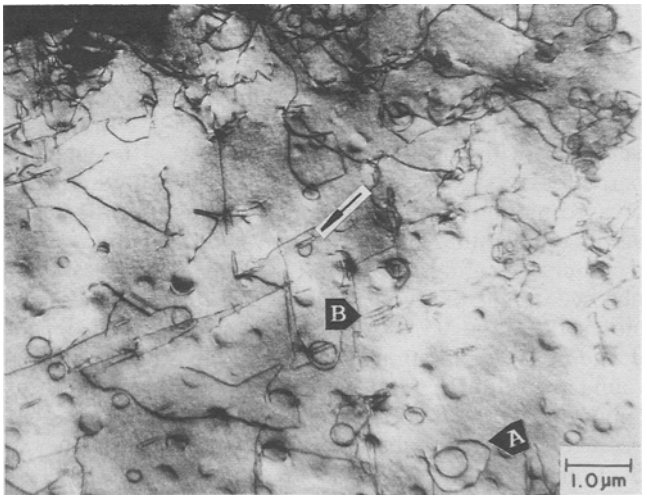

Fig. 12—Micrograph showing Orowan looping as the dominant mechanism of precipitate dislocation interaction. Intersection of loops on two different slip planes is indicated by an arrow.

the fracture surface (Figure 14(b)). Some regions also showed void coalescence (Figure 14(c)). In these specimens, it was difficult to ascertain whether the γ' particles also acted as nucleation sites.

IV. DISCUSSION AND ANALYSIS

A. *Microstructure of the Deformed Alloy*

The observed changes in the nature of the dislocation arrangement accompanying the growth of precipitates could be summarized as follows. The nonplanar dislocation arrangement in solution-annealed specimens changed to a planar arrangement with the formation of precipitates. The planar arrangement persisted as long as the γ' particles were small enough for precipitate shearing to be the predominant mode of precipitate-dislocation interaction. However, in specimens containing sufficiently large precipitates, Orowan looping became the preferred mode of interaction. In these samples, the back stress caused by the dislocation loops around the particles promoted cross slip. However, in the absence of particle shearing, there was no lowering of the resistance to subsequent dislocation motion, a factor which, otherwise, would have tended to bring about a planar arrangement. As a result, a tangled arrangement of dislocations reappeared in specimens containing large precipitates. This observed change in dislocation arrangement with increasing particle size in the aged and deformed specimens agreed well with that reported by Raynor and Silcock[10] for a PE16 alloy.

A qualitative explanation of the observed variation of the strength of the alloy with increasing average precipitate size is straightforward. A quantitative theoretical estimation is presented in Section IV–B. Assuming that the volume fraction of the precipitate phase is independent of the precipitate size, it can be surmised that the interparticle spacing increases with increasing precipitate size. When this spacing is small, the dislocations remain relatively straight as they move due to the application of external stresses. In this small precipitate–small interparticle spacing situation, precipitate shearing predominates and dislocations move in pairs in a γ' bearing alloy like MONEL K 500. When the leading dislocation of a pair cuts a precipitate, its motion is impeded by the formation of an antiphase domain boundary (APB). However, the trailing dislocation balances the APB force, and thus, the yield stress of the matrix-precipitate aggregate tends to approach that of the matrix phase. As the precipitates grow in size, the interparticle spacing increases. In this situation, the leading dislocation of a moving dislocation pair can bow when it encounters a

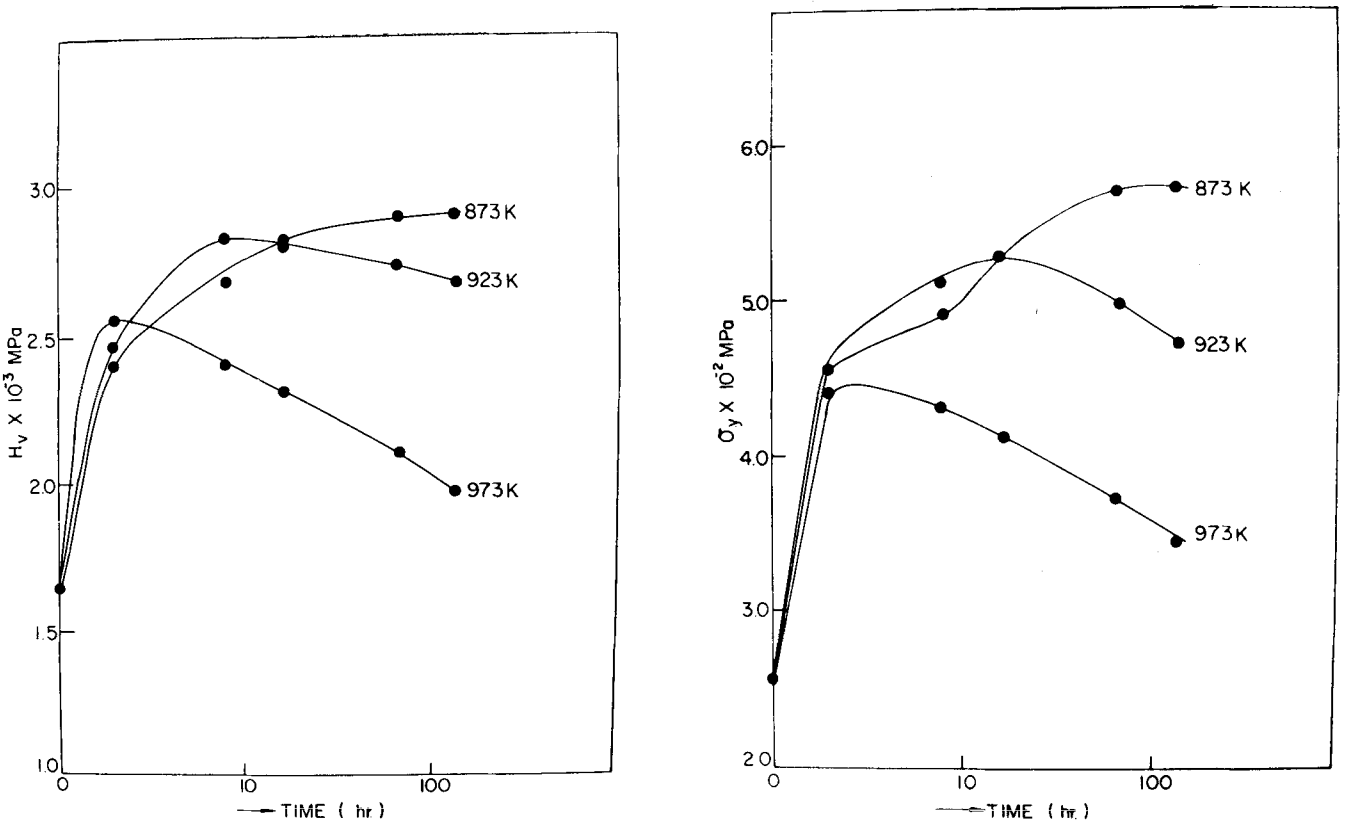

Fig. 13—Plots showing (*a*) hardness variation of aged alloys as a function of aging temperature and time and (*b*) variation of yield strength as a function of aging temperature and time.

precipitate. As a consequence, it encounters more particles than the trailing dislocation which remains relatively straight. Since the leading dislocation encounters more particles than the trailing dislocation, the former meets with greater resistance to its motion.[16] As a result, an increase in the applied stress, accompanied by a decrease in the pair width, is necessary to move the pair. The leading dislocation may either bypass the particle or shear it, depending upon which process requires smaller stress. The former process is favored as the interparticle spacing increases. Both weak and strong coupling to dislocation-precipitate interaction[17] could be seen in MONEL K 500. An illustration is given of weakly paired dislocations interacting with underaged particles (Figure 6). The average spacing between the paired dislocations was found to be about 10 to 15 times the average particle diameter and about 5 times the average interparticle spacing, in conformity with the model of weak coupling.[17] Some examples of strongly coupled dislocations can be seen in Figure 8(b).

B. *Application of Theoretical Models of Strengthening*

In most cases of precipitation hardening, in the initial stages of particle coarsening, the interparticle spacing is small and particle shearing is favored. With the progress of coarsening, as the interparticle spacing increases, looping of the precipitates becomes possible. When precipitate shearing occurs, the strengthening of the alloy can arise due to (a) coherency strain hardening, (b) surface hardening, (c) order hardening, (d) modulus hardening, and (e) stacking fault hardening. In precipitation-hardened nickel-base superalloys, strengthening primarily results from order and coherency hardening mechanisms. In order to evaluate the relative roles of the two mechanisms, the theoretically calculated values of $\Delta\tau$, the increase in the critical resolved shear stress (CRSS), has been found for each mechanism and compared with the observed values.

In MONEL K 500, the major contribution to hardening is order hardening. The other important mechanism of hardening, coherency strain hardening, is likely to make a very small contribution to the overall precipitation-hardening effect, because the coherency strain ε is extremely small (less than 0.003). At such small values of coherency strain, the coherency hardening is very small and could be neglected, as estimated by the relationship[18]

$$\Delta\tau = \alpha[G_r|\varepsilon|]^{3/2}\,[fr\mathbf{b}/2s]^{1/2} \qquad [1]$$

where α is a constant, G_r the shear modulus of the alloy (68.6 GPa), f the precipitate volume fraction, r the average particle radius, s the line tension of the dislocation, and $\mathbf{b}$ its Burgers vector.

Order hardening, the main hardening mechanism in this low misfit alloy, is brought about by the interaction of dislocations with ordered precipitates and has been

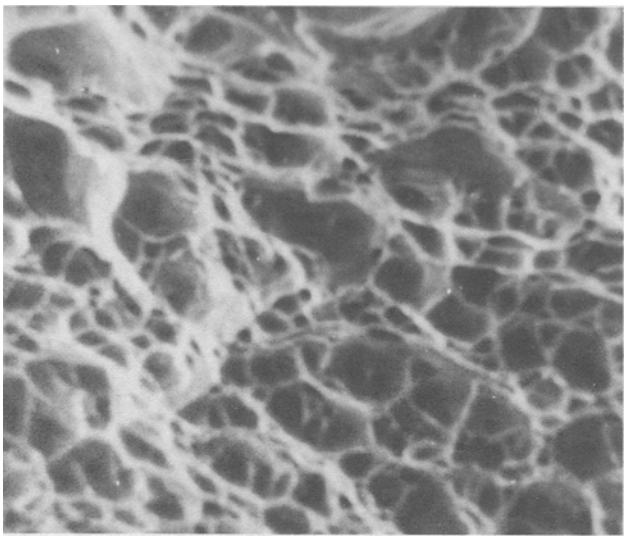

(*a*)

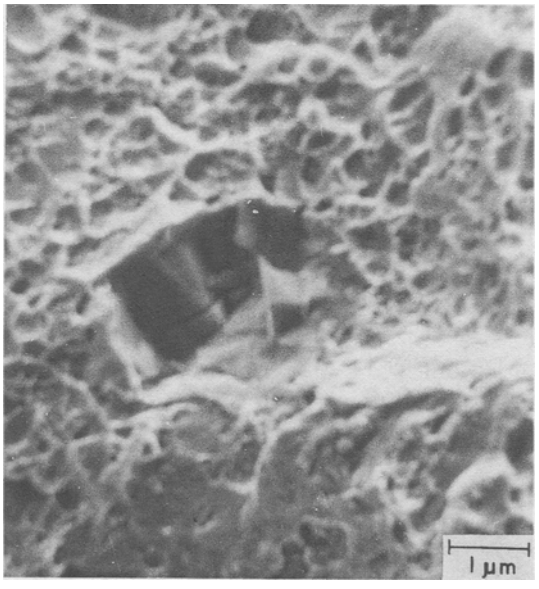

(*b*)

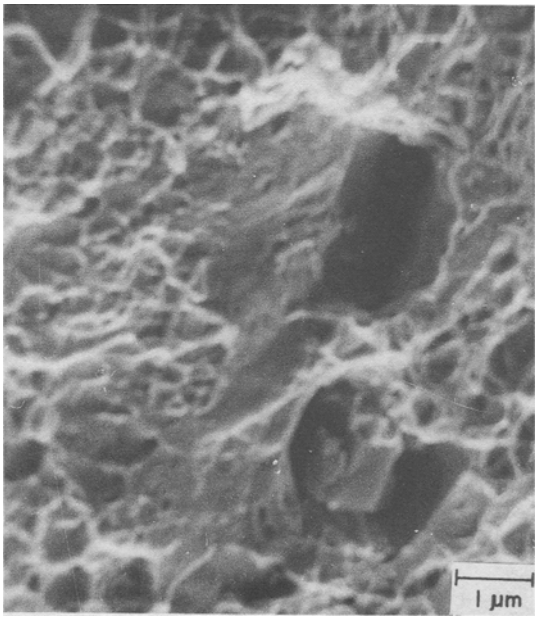

(*c*)

Fig. 14—Fractograph of (*a*) solution-treated specimen showing a bimodal size distribution of dimples, (*b*) shallower dimples at the fracture surface indicating a lower ductility at the fracture surface after aging, and (*c*) void coalescence in fractured surface of aged specimen. Carbide particles can be seen at the base of some of the dimples.

considered in three different age-hardened conditions, namely, underaged, peak aged, and overaged conditions. The precipitate dislocation interaction mechanisms corresponding to these conditions have been examined in the following sections.

1. *Underaged condition*

The major contribution to hardening in the underaged condition was due to the cutting of ordered precipitates by dislocations and the consequent creation of APB. A relationship based on a model which combines the Brown–Ham approach[2] and that of Haasen and Labusch[3] was used to calculate the CRSS required to move weakly coupled dislocation pairs cutting ordered precipitates:[4]

$$\Delta\tau = (A_1^{3/2}/2\mathbf{b})\,(rf/s)^{1/2} + A_2\gamma_1 f/2\mathbf{b} \qquad [2]$$

where $A_1 = 0.91$, $A_2 = 0.55$, and γ_1 is the APB energy of the γ' phase. The value of the line tension s was calculated by an iterative process suggested by Reppich,[19] which considers the anisotropic nature of the two-phase material.

2. *Peak-aged condition*

In the peak-aged condition, precipitation strengthening of a material hardened by shearable, "zero" misfit

ordered precipitates, would be governed solely by the shearing of the particles. This is due to the fact that the shear stress required for particle shearing is lower than the Orowan stress associated with the looping of dislocations around precipitates.[20] The increase in the flow stress brought about by precipitation hardening in the peak-aged condition was estimated by using the relationship[4]

$$\Delta\tau = \frac{\gamma_1}{2\mathbf{b}}\left\{\frac{2w_s}{(\pi w_q)^{1/2}}f^{1/2} - f\right\} \qquad [3]$$

where $w_s = 0.82$ and $w_q = 0.75$.

It is noted that Eq. [3] gives the upper limiting value for $\Delta\tau$.

3. *Overaged condition*

In the overaged condition, two processes may take place, concurrently or in succession: (1) particle cutting in slightly overaged conditions and (2) Orowan looping in substantially overaged conditions.

In a moving dislocation pair, when the first dislocation is impeded by a dislocation loop around a precipitate, the approach of the second dislocation increases the shear stress between the leading dislocation and the loop, and consequently, the particle may be sheared and the loop annihilated. Thus, planar slip may be observed in an alloy containing slightly overaged γ' particles. In the present work, the CRSS for slightly overaged alloy was estimated by using the relationship[4]

$$\Delta\tau = \frac{\mu G_r \mathbf{b}}{\pi r}\left\{\frac{f}{\pi w_q}\left(\frac{2\pi w_s \gamma_1 r}{\mu G_r \mathbf{b}^2} - 1\right)\right\}^{1/2} \qquad [4]$$

where μ is a coefficient.

The reduction in stress due to the coarsening of precipitates is compensated by the transition of dislocation pairs to single dislocations, and thus, there is a net increase in strength in the initial stages of overaging.

In the substantially overaged alloy, the interparticle spacing increased due to the coarsening of γ' particles, and the paired dislocations decomposed to single dislocations. Consequently, the precipitates were bypassed by dislocations, leaving behind a large number of shear loops around the particles. The estimate of stress in this stage was made by using the following expression:[21]

$$\Delta\tau = Y\frac{4\mathbf{b}M_{eg}}{r[(\pi w_q/f)^{1/2} - 2w_s]}\frac{[\ln\{8w_s r/R_i\}]^{3/2}}{[\ln\{r(\pi w_q/f)^{1/2}/R_i\}]^{1/2}} \qquad [5]$$

where $M_{eg} = [M_e(\Theta = 0)\cdot M_e(\Theta = \pi/2)]^{1/2}$, $M_e(\Theta = 0) = 2.73$ GPa, $M_e(\Theta = \pi/2) = 4.52$ GPa, $R_i = \mathbf{b}$, and Y is a statistical factor with a value of 0.9.

C. *Determination of APB Energy of the γ' Phase*

An estimate of the APB energy of the γ' phase was required for determining the increase in strength due to precipitation hardening while considering the mechanisms previously mentioned, except that for Orowan strengthening. Several methods have been suggested for the determination of the APB energy and in the context of precipitation these have been found to yield values which differ considerably. A few of these methods are outlined in the following sections.

1. *Minimum Orowan loop size method*

This method is based on the fact that a particle of critical size can only support a loop when the force on the dislocation arising from self-stress equals the force generated due to the creation of APB on shearing the particle.[22] The smallest observable loop is in a critical condition where these two forces just balance. The radius of such a loop can be related to the APB energy γ_1 by the following equation:[22]

$$\gamma_1 = \frac{G_r \mathbf{b}^2}{8\pi r_0}\ln\left(\frac{8r_0}{\mathbf{b}}\right)\left(\frac{2-\nu}{1-\nu}\right) \qquad [6]$$

where r_0 is the minimum loop radius and ν the Poisson's ratio.

In the present work, a large number of loops were examined in the aged and deformed specimens. These loops were examined in $+g$ and $-g$ reflecting conditions in order to allow for the displacement of electron images from dislocation centers. The minimum loop diameter was found to be about 9 nm, which yielded a value of $\gamma_1 = 0.167$ J/m^2.

This method of determining the APB energy suffers from some possible errors which are discussed in Reference 4.

2. *Dislocation-pair spacing method*

The average spacings δ were measured between dislocations in a pair lying beyond the range of influence of other dislocations. The repulsive force between the dislocations in a pair is balanced by the APB energy that each dislocation encounters.[23] The repulsive force (R') can be expressed by the following equation:[10]

$$R' = \frac{G_r \mathbf{b}^2}{2\pi\delta}\left(\frac{1 - \nu\cos^2\Theta}{1-\nu}\right) = 1/2\left(\frac{\gamma_1^{3/2} r^{1/2} f^{1/2}}{s^{1/2}} + \gamma_1 f\right) \qquad [7]$$

where Θ is the angle between the Burgers vector and the dislocation line. The average value of APB energy determined by this method was found to be $\gamma_1 = 0.185$ J/m^2. In addition to these two methods, the APB energy was also estimated by using the following equation:[19]

$$\Delta\tau_{\text{peak}} = 0.56\left(\frac{\gamma_1}{\mathbf{b}}\right)f^{1/2} \qquad [8]$$

where $\Delta\tau_{\text{peak}}$ was equated to the observed peak strength and value of APB energy found to be equal to 0.157 J/m^2. The values of the APB energy of the γ' phase determined in this study by various methods are not very different and are close to that in PE16.[4] Titanium has been found to increase the γ' APB energy in some alloys.[10] Since the titanium content of this alloy is just slightly different than that of PE16, the APB energy values are also close.

The theoretically estimated values of $\Delta\tau$ for specimens aged at 923 K in the underaged, peak-aged, and overaged conditions are shown in Figure 15, using an APB

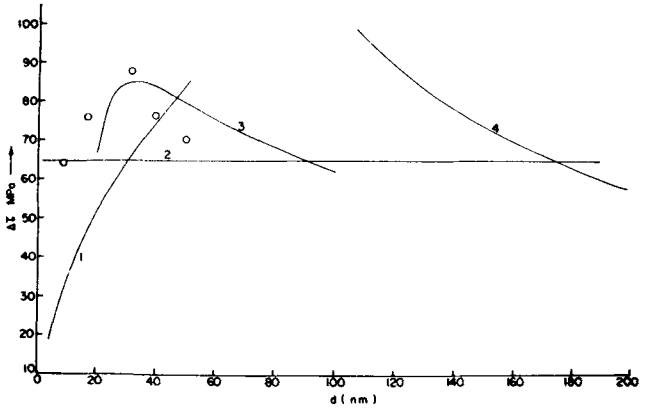

Fig. 15—Plots showing the theoretically estimated value of $\Delta\tau$ as a function of γ' particle size attributable to (1) underaged (Eq. [2]), (2) peak-aged (Eq. [3]), (3) slightly overaged (Eq. [4]), and (4) substantially overaged (Eq. [5]) conditions.

energy value of 0.16 J/m^2. Also shown are the experimentally determined values of $\Delta\tau$.

A fact of considerable significance is that the amount of solute atoms like aluminum and titanium in the γ matrix containing γ' precipitates is smaller than the solution-treated and quenched matrix which is precipitate free.[2] Titanium and aluminum are very potent solid solution strengtheners in nickel-base alloys.[18] Depletion of the matrix in these elements caused by precipitate formation is likely to bring down the strength of the matrix. Nembach and Neite[4] suggested the following relation for separating the contributions caused by solid solution hardening, τ_M, from those owing to precipitation hardening:

$$\tau_0^{3/2} = \tau_M^{3/2} + \Delta\tau^{3/2} \quad [9]$$

where τ_0 is the total strengthening and $\Delta\tau$ is the strengthening due to precipitates.

In order to accurately determine τ_M in the case of the alloy NIMONIC PE16, Nembach and Neite[4] made an alloy having the composition of the solute-depleted matrix after γ' precipitation is complete in the alloy. Such an exercise was not undertaken in the present study, since it was found that the extent of solute depletion of the matrix after complete γ' precipitation was small. The loss in strength of the matrix after precipitation was estimated by considering the solid solution strengthening effect of each element going into the precipitate individually and by adding these contributions.[24] It was found that the total loss in strength of the matrix owing to solute depletion was not substantial. This is not surprising, because the volume fraction of the γ' phase is rather small in MONEL K 500.

The agreement between the observed increase in strength and that predicted from the models was satisfactory in the small particle size regime. However, for the larger particle size range (peak-aged and overaged), the agreement was not as good, presumably because in such specimens, precipitate shearing and Orowan looping might occur concurrently. In such a situation, it would not be possible to describe the observed behavior by considering just one model, because each model assumes only one specific type of dislocation particle interaction.

D. *Work Hardening*

The rate of work hardening in the presence of precipitates was found to be higher than that obtained in the case of the precipitate-free (solution-treated) matrix and increased with increasing precipitate size. In specimens where cutting of particles was noticed, the increase in work hardening rate was small. The enhancement in work hardening rate with increasing particle size, even in specimens where particle shearing occurred, was presumably owing to the fact that the passage of dislocations through a particle reduced that particle's diameter, making the passage of the next pair easier. The relative reduction in diameter for a small particle is known to be larger than that for a large particle.[17]

In specimens where Orowan looping occurred, work hardening was found to be very strong. A straightforward explanation for this is the gradual reduction in the effective interparticle spacing with the formation of loops around precipitates, making passage of dislocations progressively difficult.[17]

E. *Fracture*

A correlation between the microstructure and the appearance of the fracture surfaces obtained by fracturing the specimens in tension is discussed in this section. The fracture surfaces were found to be dimpled in solution-treated as well as in solution-treated and aged specimens, which was indicative of the occurrence of ductile fracture in all these specimens. Ductile fracture by dimple formation involves three stages: void nucleation, void growth, and void coalescence.[25,26] Voids have generally been found to nucleate at particle-matrix interfaces. With this point in view, nucleation of voids at the interfaces of different types of particles, such as carbide and γ' precipitates, was examined in different specimens. Void growth and coalescence were also likely to be influenced by the morphology of the particles.[27]

It was suggested earlier that some second-phase particles act as nucleation sites for voids only if their size is greater than a critical size.[28] The nature of the particle is also important; a precipitate-matrix interface is likely to be more secure than the interface between an inclusion and the matrix.

Specimens containing very large γ' particles also showed larger dimples. The dimples were much shallower than those seen in solution-treated specimens. Some flat regions indicative of shear could be seen (Figure 14(b)). The fracture surface also showed some large ridges and furrows. The presence of carbide particles at the base of larger dimples was indicative of the fact that the primary carbide particles were effective nucleating agents. The $M_{23}C_6$-type carbides which formed at the grain boundaries did not promote intergranular fracture. This is not surprising in view of the fact that such carbides have been found to cause intergranular failure only if these are present in the form of a continuous film at the grain boundaries.[29]

V. CONCLUSIONS

1. Significant age hardening occurs in MONEL K 500 due to the precipitation of the γ' phase.

2. When the alloy is deformed in the underaged condition, there is a pronounced tendency for dislocations to move in pairs, and particle shearing is the predominant mode of dislocation-precipitate interaction. The observed interdislocation spacing is in reasonably good agreement with that predicted on the basis of weak coupling models.
3. Deformation of the peak-aged alloy involves both particle shearing and looping of dislocations around precipitates. Strongly coupled dislocation pairs could be observed in the peak-aged alloy.
4. In the overaged alloys, looping of dislocations around precipitates is the primary mechanism of dislocation-precipitate interaction. A transition from paired dislocations to single dislocations is associated with the looping process.
5. While slip is predominantly planar in the underaged alloy, cross slip occurs in the overaged alloy, leading to complex slip interactions and a concomitant enhancement in work hardening.
6. The agreement between the observed increase in strength and that predicted on the basis of relevant models is the most satisfactory in the small precipitate size regime.

ACKNOWLEDGMENTS

It is a pleasure to acknowledge the benefit of several discussions the authors had with Dr. M. Sundararaman, Dr. J.K. Chakravartty, and Dr. S. Banerjee. The authors are grateful to Dr. S. Banerjee, Head, Metallurgy Division, for his constant encouragement throughout the course of this work. Thanks are due to Mr. R.T. Savalia and Mrs. J. Gupta for assistance in experimentations.

REFERENCES

1. G.K. Dey and P. Mukhopadhyay: *Mater. Sci. Eng.*, 1986, vol. 84, pp. 177-89.
2. L.M. Brown and R.K. Ham: in *Strengthening Methods in Crystals*, A. Kelly and R.B. Nicholson, eds., Applied Science Publication Ltd., London, 1971, pp. 9-22.
3. P. Haasen and R. Labusch: *Proc. 5th Int. Conf. on the Strength of Metals and Alloys*, Pergamon Press, Toronto, 1979, vol. 1, p. 639.
4. E. Nembach and G. Neite: *Prog. Mater. Sci.*, 1985, vol. 29, pp. 177-319.
5. U.F. Kocks: *Mater. Sci. Eng.*, 1977, vol. 27, pp. 291-98.
6. P.B. Hirsch and F.J. Humphrey: *Physics of Strength and Plasticity*, A.S. Argon, ed., MIT Press, Cambridge, MA, 1969, pp. 89-216.
7. P.C.J. Gallagher: *Metall. Trans.*, 1970, vol. 1, pp. 2429-61.
8. P.S. Kotval: *Trans. AIME*, 1968, vol. 242, p. 1651.
9. B.E.P. Beeston and L.K. France: *J. Int. Met.*, 1968, vol. 96, pp. 105-07.
10. D. Raynor and J.M. Silcock: *Met. Sci. J.*, 1970, vol. 4, pp. 121-29.
11. H. Gleiter: *Acta Metall.*, 1968, vol. 16, pp. 455-64.
12. L. Delehouzce and A. Deruyttere: *Acta Metall.*, 1967, vol. 15, pp. 728-34.
13. A. Gyster, G. Lutejering, and V. Gerold: *Acta Metall.*, 1974, vol. 22, pp. 901-09.
14. L.K. Singhal and J.W. Martin: *Acta Metall.*, 1968, vol. 16, pp. 947-53.
15. A.W. Thompson and P.F. Weihrauch: *Scripta Metall.*, 1976, vol. 10, pp. 205-10.
16. R.J. Taut and B. Ralph: *Phil. Mag.*, 1974, vol. 30, pp. 1379-94.
17. V. Martens and E. Nembach: *Acta Metall.*, 1975, vol. 23, pp. 149-53.
18. E. Nembach: *Scripta Metall.*, 1981, vol. 18, pp. 105-10.
19. B. Reppich: *Acta Metall.*, 1982, vol. 30, pp. 87-94.
20. W. Huther and B. Reppich: *Z. Metallkd.*, 1978, vol. 69, pp. 628-34.
21. D.J. Bacon, U.F. Kocks, and R.O. Scattergood: *Phil. Mag.*, 1973, vol. 28, pp. 1241-63.
22. L.M. Brown: *Phil. Mag.*, 1964, vol. 10, pp. 441-66.
23. J. Friedel: *Dislocations*, Pergamon Press, 1964, p. 38.
24. N.S. Stoloff: in *The Superalloys*, C.T. Sims and W.C. Hagel, eds., John Wiley and Sons, New York, NY, pp. 79-112.
25. S. Banerjee and R. Krishnan: *Acta Metall.*, 1978, vol. 26, pp. 1815-31.
26. P.F. Thomason: *J. Inst. Met.*, 1968, vol. 96, pp. 360-65.
27. G. Le Roy, J.D. Embury, G. Edward, and M.F. Ashby: *Acta Metall.*, 1981, vol. 29, pp. 1509-22.
28. L.M. Brown and D. Embury: *Proc. 3rd Int. Conf. on Strength of Metals and Alloys*, Cambridge, United Kingdom, 1973, pp. 164-69.
29. G.K. Dey, D. Srivastava, A. Shaju, M. Sundararaman, and P. Mukhopadhyay: *Mater. Sci. Eng.*, 1989, vol. 119, pp. 175-89.